biomimetics

MDPI

Article

Biocompatibility and Antibacterial Potency of a Gentamicin-Loaded 3D-Printed Porcine ECM-Derived Collagen Scaffold for Infected Soft Tissue Reconstruction: An In Vitro Study

Min Ji Kim, Hyung Gi Kim, Seung Hee Hong, Eun Hee Han, Su Jin Lim and Il Jae Lee *

Department of Plastic and Reconstructive Surgery, Ajou University School of Medicine, Suwon 16499, Republic of Korea; minjikim1031@naver.com (M.J.K.)
* Correspondence: i00325@live.co.kr; Tel.: +82-31-219-5614

Abstract

Reconstruction of infected soft tissue defects requires a biomaterial providing structural support for tissue regeneration and sustained local infection control. We developed a gentamicin-loaded 3D-printed porcine extracellular matrix (ECM)-derived collagen scaffold and evaluated its in vitro biocompatibility and antibacterial potency. Porcine type I collagen scaffolds were 3D-bioprinted, stabilized by chemical (1-ethyl-3-(3-dimethylaminopropyl)carbodiimide/N-hydroxysuccinimide, EDC/NHS) or physical (dehydrothermal) crosslinking, and loaded with gentamicin. Six groups differing in fabrication, crosslinking, and gentamicin loading, including conventional sponges, were compared. Cell adhesion at 24 h and metabolic activity, proliferation, and infiltration over 7 days were assessed in L929 fibroblasts, and gentamicin potency by microbiological assay. Compared with sponges, 3D-printed scaffolds showed up to 1.46-fold higher 24 h adhesion, significantly higher proliferation, and up to 3.37-fold deeper infiltration ($p < 0.001$). Chemical crosslinking supported higher day-7 metabolic activity without and with gentamicin (2.05 ± 0.07 and 2.15 ± 0.21) than physical crosslinking ($p < 0.05$). Gentamicin incorporation did not impair cellular responses to the 3D-printed scaffolds, and antibacterial potency was preserved after fabrication. The scaffold showed favorable preliminary cytocompatibility and preserved antibacterial potency, with EDC/NHS as a promising crosslinking method. These findings support its potential as an implantable biomaterial integrating structural support with expected local antibacterial activity.

Keywords: extracellular matrix; collagen type I; printing; three-dimensional; gentamicins; tissue scaffolds; reconstructive surgical procedures

Check for updates

Academic Editors: Hermann Ehrlich and Bo Su

Received: 16 October 2026
Revised: 6 November 2026
Accepted: 14 November 2026
Published: 16 November 2026

Copyright: © 2026 by the authors. Licensee MDPI, Basel, Switzerland. This article is an open access article distributed under the terms and conditions of the Creative Commons Attribution (CC BY) license.

1. Introduction

Soft tissue defects complicated by infection represent one of the most challenging problems in reconstructive surgery [1,2]. Even when biocompatibility is assured, successful implantation cannot be achieved unless the associated infection is adequately controlled. Bacterial colonization at the surgical site leads to implant failure, wound dehiscence, and prolonged hospitalization, ultimately compromising patient outcomes [1].

In response to this unmet need, considerable research efforts have been directed toward the development of antibiotic-loaded medical devices [3,4]. Among these, resorbable lyophilized (freeze-dried) collagen sponges or fleeces impregnated with gentamicin sulfate are among the few formulations that have reached clinical use, primarily in cardiac and

abdominal surgery [5]. Multiple randomized controlled trials and meta-analyses have substantiated their clinical efficacy in significantly reducing surgical site infections, particularly in gastrointestinal and cardiac surgeries [6,7]. Despite their proven antimicrobial efficacy, conventional sponges remain limited by their random pore networks and uncontrolled degradation kinetics, providing minimal structural support for active cellular ingrowth and tissue reconstruction [4].

Beyond these device-related limitations, a more fundamental clinical challenge lies in the patient population itself. In reconstructive practice, a substantial proportion of infected soft tissue defects occur in patients whose underlying condition precludes definitive surgical management. Patients with significant comorbidities, including diabetes mellitus, peripheral vascular disease, or immunocompromised states, frequently fail to achieve reliable healing through surgery alone. This limitation also applies to patients suffering from recalcitrant wounds that persist despite repeated operative interventions. For these challenging cases, active conservative management serves as a critical alternative to conventional surgical approaches. Achieving successful healing through this strategy requires a biomimetic scaffold capable of tissue substitution to guide structural regeneration. Concurrently, because conservative healing involves prolonged wound exposure, sustained and effective local infection control is imperative to protect the vulnerable healing bed throughout the extended treatment period. In this context, the ideal implantable material should serve a dual function, acting as a scaffold that supports cellular attachment, migration, proliferation, and tissue remodeling, while simultaneously delivering local antimicrobial agents to prevent or treat infection at the implantation site [3,4,8]. However, achieving this balance presents significant developmental challenges. The incorporation of antibiotics must not compromise the scaffold's structural integrity, pore architecture, or cytocompatibility, all of which are critical for successful tissue regeneration [9,10].

Type I collagen, the principal structural protein of the native extracellular matrix (ECM), has been widely investigated as an ECM-mimetic scaffold material for tissue regeneration owing to its biocompatibility, biodegradability, and low immunogenicity [11–14]. Crosslinking further stabilizes the collagen matrix, improving mechanical integrity and controlled degradation kinetics favorable for sustained drug release [4,15,16]. To overcome the structural limitations of conventional matrices, three-dimensional (3D) bioprinting enables layer-by-layer fabrication with precise control over pore geometry, interconnectivity, and scaffold dimensions, which govern nutrient diffusion, cellular ingrowth, and ultimately the quality of tissue regeneration [17–19]. We therefore hypothesized that loading such a 3D-printed ECM-derived collagen scaffold with an antibiotic would provide antibacterial activity while preserving its structural and biological properties favorable for tissue repair.

In this context, we prepared gentamicin-loaded 3D-printed scaffolds from porcine ECM-derived type I collagen. Building on clinically used gentamicin–collagen sponges and 3D-printed collagen constructs, this study compared conventional collagen sponges with chemically or physically crosslinked 3D-printed scaffolds, with and without gentamicin, all prepared from the same collagen source, so that cellular responses could be compared across fabrication methods, crosslinking methods, and gentamicin loading within a single material system. Initial cell adhesion, metabolic activity, proliferation, and infiltration of L929 fibroblasts and the gentamicin content of the scaffold were evaluated.

2. Materials and Methods

2.1. Scaffold Fabrication

2.1.1. Collagen Bioink Preparation

Porcine ECM-derived type I collagen (MS Bio Co., Ltd., Seongnam, Republic of Korea) was extracted from porcine skin of animals aged less than 12 months through a standard-

ized extraction and purification process, including decellularization and removal of non-collagenous components [20–22]. The scaffolds therefore consisted of purified ECM-derived type I collagen rather than a multicomponent decellularized ECM and are hereafter referred to as ECM-derived collagen scaffolds. The purified collagen was neutralized (NaOH/HCl), mixed with phosphate buffer to induce fibrillization, adjusted to 6% (w/v), stirred for 24 h, and degassed under refrigeration.

2.1.2. 3D Printing

Scaffolds were printed using a custom-built, temperature-controlled pneumatic extrusion bioprinter with a 25-gauge nozzle at a deposition speed of 25 mm/s and a layer height of 0.15 mm, in a grid pattern alternating at 0° and 90° [17], and were subsequently lyophilized.

2.1.3. Crosslinking

Chemical crosslinking was performed using 1-ethyl-3-(3-dimethylaminopropyl) carbodiimide/N-hydroxysuccinimide (EDC/NHS) at a 4:1 molar ratio for 4 h at room temperature, followed by washing with Na_2HPO_4 solution and purified water; removal of residual EDC was confirmed by a residual EDC assessment [15,23]. Physical crosslinking was performed by dehydrothermal treatment under vacuum at 105 °C [16,24].

2.1.4. Gentamicin Loading and Sterilization

After crosslinking (where applicable), gentamicin sulfate was incorporated via immersion in a 2.0% (w/v) gentamicin sulfate solution for 1 h at room temperature under static conditions (target loading: 2 mg/cm^2 of scaffold area), followed by secondary freeze-drying, sterile packaging, and ethylene oxide sterilization with aeration [4,10]. Other loading methods, such as adding gentamicin to the ink before printing, were not evaluated.

2.2. Experimental Group

Scaffolds were divided into six experimental groups according to three factors: fabrication method (3D-printed vs. freeze-dried sponge), crosslinking method (chemical vs. physical, applicable to 3D-printed scaffolds only; Section 2.1.3), and gentamicin loading (loaded vs. non-loaded) (Figure 1).

The six groups were as follows: (i) collagen sponge without gentamicin (Sponge), (ii) collagen sponge loaded with gentamicin (Sponge+G), (iii) chemically crosslinked 3D-printed ECM-derived collagen scaffold without gentamicin (3D-Chem), (iv) chemically crosslinked 3D-printed ECM-derived collagen scaffold loaded with gentamicin (3D-Chem+G), (v) physically crosslinked 3D-printed ECM-derived collagen scaffold without gentamicin (3D-Phys), and (vi) physically crosslinked 3D-printed ECM-derived collagen scaffold loaded with gentamicin (3D-Phys+G) (Table 1).

Table 1. Classification of experimental groups according to fabrication method, crosslinking method, and gentamicin loading status.

Group	Fabrication	Crosslinking	Gentamicin
Sponge	Freeze-dried	–	–

Table 1. *Cont.*

Group	Fabrication	Crosslinking	Gentamicin
Sponge+G	Freeze-dried	–	+
3D-Chem	3D-printed	Chemical	–
3D-Chem+G	3D-printed	Chemical	+
3D-Phys	3D-printed	Physical	–
3D-Phys+G	3D-printed	Physical	+

3D-Chem, chemically crosslinked 3D-printed ECM-derived collagen scaffold; 3D-Phys, physically crosslinked 3D-printed ECM-derived collagen scaffold; +G, gentamicin-loaded; and ECM, extracellular matrix. In the crosslinking column, – indicates no crosslinking. In the gentamicin column, + and – indicate the presence and absence of gentamicin, respectively.

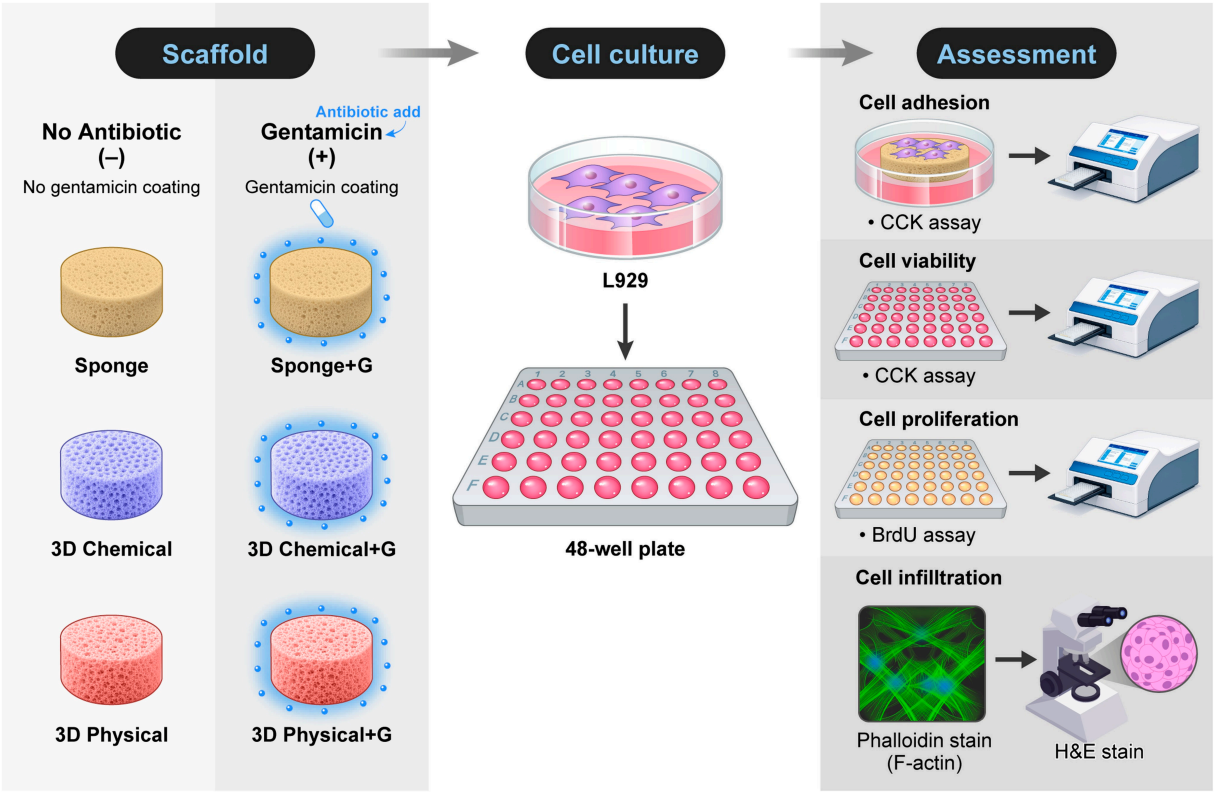


Figure 1. Schematic overview of scaffold fabrication and the in vitro experimental design. Porcine ECM-derived type I collagen scaffolds were prepared as conventional freeze-dried sponges (control) or 3D-printed constructs crosslinked either chemically (EDC/NHS) or physically (vacuum dehydrothermal treatment). Six distinct groups (with or without gentamicin) were established and seeded with L929 fibroblasts for subsequent in vitro assays, including cell adhesion, metabolic activity, proliferation, and three-dimensional infiltration.

2.3. In Vitro Analysis

All subsequent cell adhesion, metabolic activity, proliferation, and infiltration analyses were performed using these scaffold groups. L929 mouse fibroblast cells were maintained in DMEM supplemented with 10% FBS and 1% penicillin–streptomycin at 37 °C with 5% CO_2, seeded onto scaffolds preconditioned in complete culture medium for 1 h at 37 °C, at a density of 3×10^4 cells per scaffold. After a 24 h adhesion period, the scaffolds were transferred to new culture plates to remove non-adherent cells, and this time point was designated as day 0. Separate scaffolds were used for each assay and time point.

2.3.1. Cell Adhesion and Metabolic Activity Assays

Cell adhesion was evaluated qualitatively by calcein-AM fluorescence imaging (2 μM; Invitrogen, Waltham, MA, USA) and quantitatively by Cell Counting Kit-8 (CCK-8) colorimetric assay (EZ-Cytox, DoGenBio Co., Seoul, Republic of Korea), with absorbance measured at 450 nm and background from cell-free scaffolds subtracted. Because CCK-8 measures cellular dehydrogenase activity, the CCK-8 absorbance at 24 h (day 0) was used as an indirect, metabolic activity-based indicator of cell adhesion rather than a direct measure of adhesion or cell number. Metabolic activity was subsequently assessed at days 0, 3, and 7 using the same CCK-8 assay; at each time point, scaffolds were rinsed with PBS, incubated with CCK-8 reagent for 1 h, and activity ratios were calculated by dividing each value at days 3 and 7 by the mean day-0 value of the same group.

2.3.2. Cell Proliferation Assay

Cell proliferation was quantified at days 0, 3, and 7 using a 5-bromo-2′-deoxyuridine (BrdU) incorporation assay (Cell Proliferation ELISA BrdU, Roche, Mannheim, Germany). BrdU labeling solution (final concentration, 10 μM) was added to the culture medium for 2 h at 37 °C, followed by fixation and processing according to the manufacturer's protocol. Absorbance was measured at 450/690 nm, background signals from cell-free scaffolds were subtracted, and proliferation ratios were calculated by dividing each value at days 3 and 7 by the mean day-0 value of the same group.

2.3.3. Cell Infiltration Analysis

Cell infiltration was evaluated after 7 days of culture by two methods. For fluorescence analysis, scaffolds were stained with Alexa Fluor 488-phalloidin and DAPI, and penetration depth was measured by confocal z-stack imaging (Celldiscoverer7 with LSM 900, ZEISS, Jena, Germany). For histological evaluation, H&E-stained cross-sections were imaged using a slide scanner (Axioscan Z1, ZEISS), and infiltration depth was quantitatively measured from the scaffold surface. Three scaffolds per group were analyzed. Penetration depth was defined as the distance from the upper scaffold surface to the deepest identifiable infiltrating cells along the depth direction, and the reported values represent mean penetration depths rather than a single maximum value.

2.3.4. Gentamicin Content Assay

The gentamicin content of the 3D-Chem+G scaffold was determined using the cylinder-plate microbiological assay of the Korean Pharmacopoeia [25], with *Staphylococcus epidermidis* ATCC 12228 as the test organism (inoculum adjusted to a transmittance of 50 ± 10%). The scaffold was extracted in 50 mL of 0.1 mol/L phosphate buffer (pH 8.0) for 4 h at room temperature with shaking (120 rpm), and the extract and a gentamicin sulfate reference standard were diluted with the same buffer to high and low concentrations of 4 and 1 μg/mL; the nominal concentrations of the extract were calculated from the target loading (2 mg/cm^2) and the specimen area. Each solution (100 μL) was applied to cylinders on seeded antibiotic medium No. 11 plates (five plates), which were incubated at 32–37 °C for 16–20 h. The inhibition zone diameters of the extract were compared with those of the reference standard, and the gentamicin content was expressed as a percentage of the target loading (acceptance range, 90–110%).

2.4. Scaffold Characterization

The surface morphology and mechanical properties of the 3D-Chem+G scaffold were characterized. Surface morphology was examined by scanning electron microscopy (SEM; VEGA3, TESCAN, Brno, Czech Republic) at an accelerating voltage of 10 kV and magni-

fications of ×50 and ×100 after platinum sputter coating, and the opening dimensions of four pores were measured in the vertical and horizontal directions on a representative ×100 image (eight measurements). Uniaxial tensile testing was performed on three specimens ($n = 3$) using a universal testing machine (Instron 3367, Instron, Norwood, MA, USA) with a 500 N load cell at a crosshead speed of 2 mm/min and a grip-to-grip distance of 15 mm under controlled conditions (23 ± 2 °C, 45 ± 5% relative humidity), and the maximum tensile load was recorded. Enzymatic resistance was evaluated by incubating 15 × 15 mm specimens ($n = 3$) in 10 mL of porcine trypsin solution (2000 U/mL in 0.1 mol/L ammonium bicarbonate, pH 7.4) at 37 ± 2 °C and 50 rpm for 24 ± 2 h, followed by visual comparison with specimens incubated in the buffer alone. In addition, sponge and 3D-printed scaffolds were immersed in culture medium and photographed at days 30, 80, and 88 to assess their macroscopic structural stability.

2.5. Statistical Analysis

Each assay was performed using three separate scaffolds per group at each time point ($n = 3$), and different scaffolds were used for each assay and time point; thus, n represents the number of scaffolds rather than repeated measurements of a single scaffold. All quantitative data are presented as mean ± standard deviation. Normal distribution was confirmed using the Shapiro–Wilk test. Statistical analyses were performed using SPSS Statistics version 29 (IBM Corp., Armonk, NY, USA). Because separate scaffolds were used at each time point and values were normalized to day 0, groups were compared separately at each time point using one-way analysis of variance (ANOVA) followed by Tukey's post hoc test; changes over time were described but not tested statistically. A p-value of less than 0.05 was considered statistically significant.

3. Results

3.1. Cellular Responses of 3D-Printed Scaffolds Compared with Conventional Sponges

To evaluate the impact of scaffold design, we compared 3D-printed scaffolds with conventional freeze-dried collagen sponges (Table 1). In the CCK-8 analysis at 24 h, the non-loaded 3D-printed scaffolds, 3D-Chem (0.28 ± 0.03) and 3D-Phys (0.29 ± 0.01), showed significantly higher adhesion than the Sponge control group (0.22 ± 0.02) (both $p < 0.001$; Table 2, Figure 2A). A similar difference was observed in the antibiotic-loaded cohorts, where the 3D-Phys + G group (0.31 ± 0.01) exhibited significantly greater adhesion than both the Sponge control ($p < 0.001$) and the 3D-Phys group ($p = 0.005$; Table 2, Figure 2A).

Table 2. Quantitative assessment of initial cell adhesion (CCK-8 absorbance at 24 h) and metabolic activity in L929 mouse fibroblasts among experimental groups.

Group	Cell Adhesion (Absorbance at 24 h)	Metabolic Activity (Relative to Day 0, at Day 7)
Sponge	0.22 ± 0.02	2.89 ± 0.35
Sponge+G	0.24 ± 0.01 [a]	2.01 ± 0.41 [b]
3D-Chem	0.28 ± 0.03 [b]	2.05 ± 0.07 [b]
3D-Chem+G	0.23 ± 0.01 [c]	2.15 ± 0.21 [b]
3D-Phys	0.29 ± 0.01 [b]	1.78 ± 0.11 [b]
3D-Phys+G	0.31 ± 0.01 [b,d]	1.53 ± 0.04 [b]

Values are presented as mean ± standard deviation ($n = 3$ per group); statistical comparisons were performed using one-way ANOVA followed by Tukey's post hoc test. [a] $p < 0.05$ vs. Sponge; [b] $p < 0.001$ vs. Sponge; [c] $p < 0.001$ vs. 3D-Chem; and [d] $p < 0.05$ vs. 3D-Phys. 3D-Chem, chemically crosslinked 3D-printed ECM-derived collagen scaffold; 3D-Phys, physically crosslinked 3D-printed ECM-derived collagen scaffold; +G, gentamicin-loaded; and ECM, extracellular matrix.

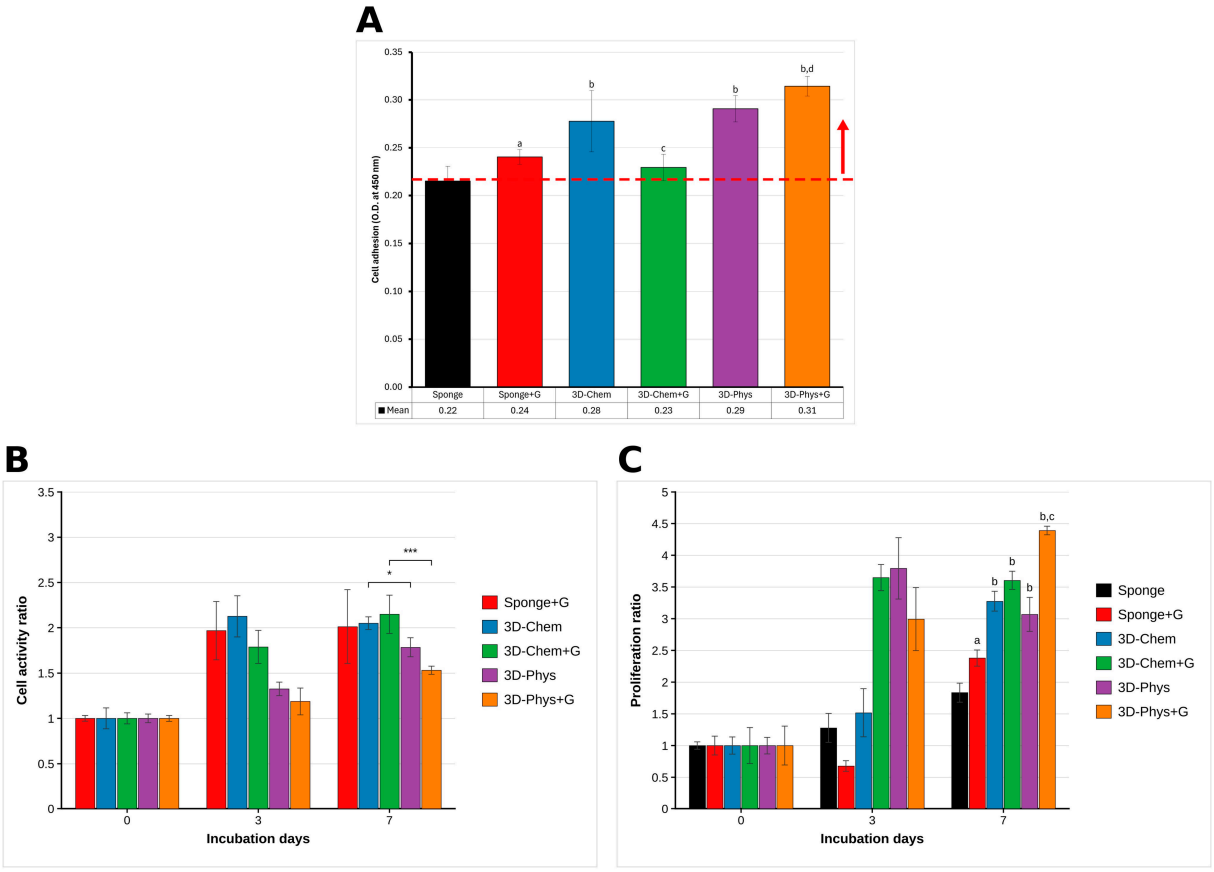


Figure 2. Cellular responses of the scaffold groups. (**A**) Cell adhesion at day 0 (24 h after seeding) measured by CCK-8 assay (O.D. at 450 nm). The red dashed line represents the mean OD value of the Sponge group, and the red arrow indicates increased cell adhesion relative to this reference. (**B**) Cell metabolic activity at days 0, 3, and 7 assessed by CCK-8 assay, expressed as the cell activity ratio normalized to day 0. (**C**) Cell proliferation at days 0, 3, and 7 evaluated by BrdU assay, expressed as the proliferation ratio normalized to day 0. All 3D-printed groups demonstrated higher proliferation than the sponge controls at day 7. Data are presented as mean ± standard deviation ($n = 3$ per group and time point). Letters in (**A**,**C**) indicate significant differences as defined in Tables 2 and 3, respectively, and * $p < 0.05$ and *** $p < 0.001$ indicate differences between the indicated groups in (**B**).

Table 3. Comparative analysis of proliferation and three-dimensional infiltration of L929 cells within scaffolds among experimental groups.

Group	Cell Proliferation (BrdU, Relative to Day 0, at Day 7)	Infiltration Depth (μm) (Confocal Z-Stack Analysis)
Sponge	1.84 ± 0.15	151.33 ± 44.38
Sponge+G	2.38 ± 0.13 [a]	195.33 ± 23.56
3D-Chem	3.28 ± 0.16 [b]	426.00 ± 110.57 [b]
3D-Chem+G	3.60 ± 0.14 [b]	467.33 ± 102.85 [b]
3D-Phys	3.07 ± 0.27 [b]	396.67 ± 96.04 [b]
3D-Phys+G	4.39 ± 0.07 [b,c]	510.00 ± 82.81 [b,c]

Values are presented as mean ± standard deviation ($n = 3$ per group); statistical comparisons were performed using one-way ANOVA followed by Tukey's post hoc test. [a] $p < 0.05$ vs. Sponge; [b] $p < 0.001$ vs. Sponge; and [c] $p < 0.05$ vs. 3D-Phys. 3D-Chem, chemically crosslinked 3D-printed ECM-derived collagen scaffold; 3D-Phys, physically crosslinked 3D-printed ECM-derived collagen scaffold; +G, gentamicin-loaded; ECM, extracellular matrix; and BrdU, 5-bromo-2′-deoxyuridine.

By day 7, the 3D-printed groups also showed higher cell proliferation and deeper three-dimensional infiltration than the sponge groups. Compared to the Sponge group

(1.84 ± 0.15), all 3D-printed groups showed significantly higher BrdU incorporation ($p < 0.001$), reaching 3.28 ± 0.16 fold for 3D-Chem and peaking at 4.39 ± 0.07 for 3D-Phys+G (Table 3, Figure 2C). Notably, while cells in the Sponge group remained near the surface (151.33 ± 44.38 µm), confocal Z-stack analysis showed significantly deeper cell infiltration into the 3D-printed scaffolds (3D-Chem: 426.00 ± 110.57 µm; 3D-Chem+G: 467.33 ± 102.85 µm; $p < 0.001$; Table 3, Figure 3A). In H&E sections, infiltration was deeper in the 3D-Chem+G, 3D-Phys, and 3D-Phys+G groups than in the Sponge group, but not in the 3D-Chem group (Figure 3B and Table S1).

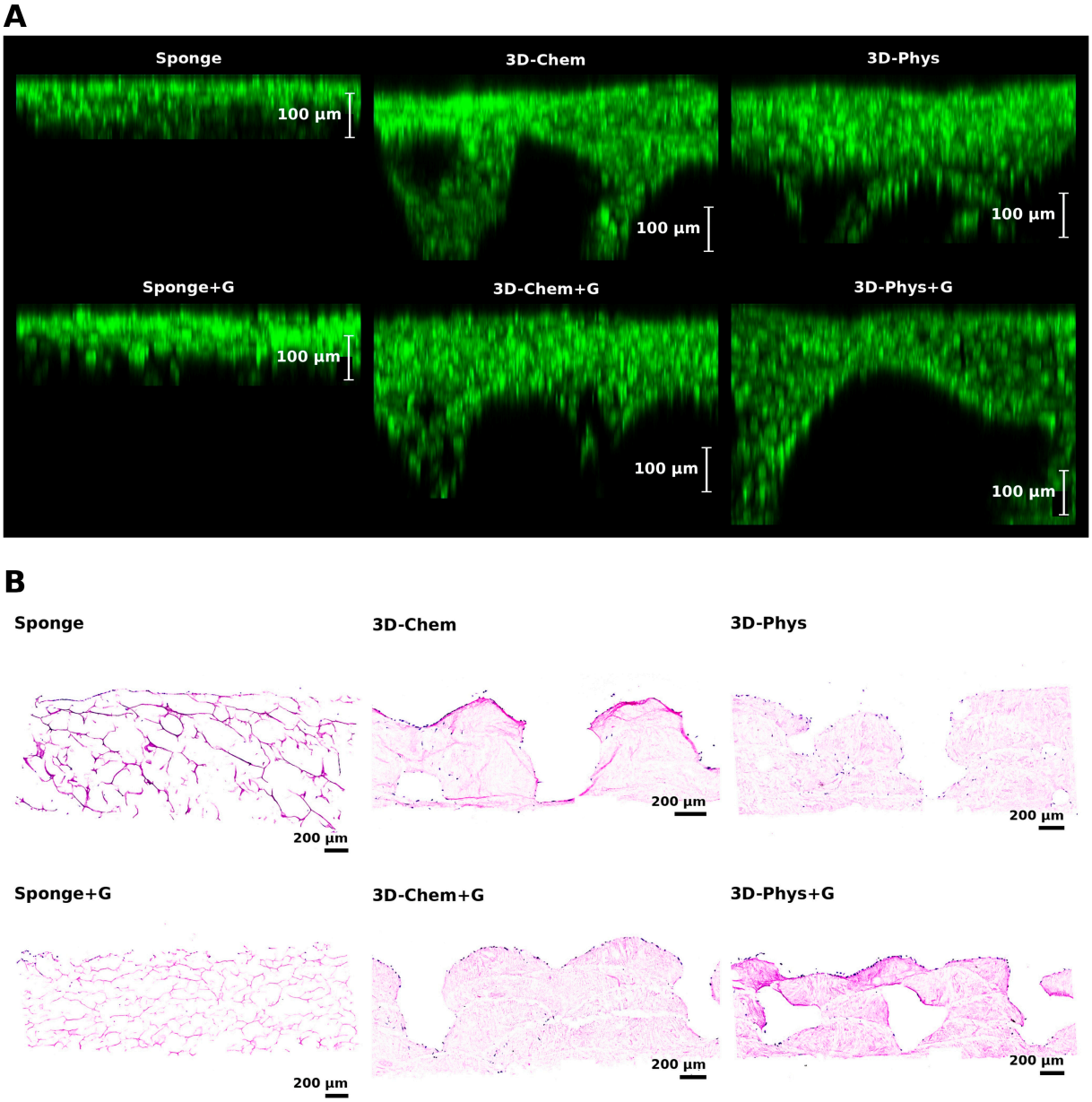


Figure 3. Architectural evaluation of three-dimensional cell infiltration. Cross-sectional visualization of cellular penetration into the scaffold groups at day 7. (**A**) Representative confocal Z-stack images of phalloidin-stained cells (green fluorescence). The sponge groups (Sponge, Sponge+G) showed cells confined primarily to the scaffold surface, whereas all 3D-printed groups exhibited deeper cellular penetration, with up to 3.37-fold greater mean penetration depth than the sponge controls. (**B**) Representative H&E cross-sectional images. The sponge groups displayed a random, closed pore structure, while the 3D-printed groups showed well-defined, interconnected pore channels.

3.2. Evaluation of Cell Metabolic Activity and Proliferation According to Crosslinking Methods

While both crosslinking strategies successfully preserved the 3D grid structures after fabrication, they induced distinct cellular response profiles over the 7-day culture period. At day 7, the cell metabolic activity of the chemically crosslinked groups was significantly higher and better preserved than that of the physically crosslinked groups. Specifically, the metabolic activity ratio reached 2.05 ± 0.07 for 3D-Chem compared to 1.78 ± 0.11 for 3D-Phys ($p = 0.040$), and 2.15 ± 0.21 for 3D-Chem+G compared to 1.53 ± 0.04 for 3D-Phys+G ($p < 0.001$; Table 2, Figure 2B). The Sponge group showed the highest day-7 relative ratio (2.89 ± 0.35; Table 2), which may partly reflect normalization to its lowest day-0 value (0.22 ± 0.02).

In contrast, the physically crosslinked constructs demonstrated contrasting trends between their metabolic activity and proliferation rates at the final time point. The 3D-Phys+G group exhibited the highest values among all experimental groups in both cell proliferation (4.39 ± 0.07; Table 3, Figure 2C) and structural infiltration depth (510.00 ± 82.81 µm; Table 3, Figure 3A). However, this high proliferation and deep infiltration were not accompanied by a correspondingly high CCK-8 signal, as the same group showed the lowest relative day-7 metabolic activity ratio (1.53 ± 0.04) among all tested cohorts (Table 2, Figure 2B). Because the CCK-8 and BrdU assays measure different cellular processes and were normalized separately, these values should not be interpreted as differences in cell number or survival.

3.3. Cytocompatibility of Gentamicin-Loaded Scaffolds

The incorporation of gentamicin sulfate to provide antibacterial activity did not compromise the baseline cytocompatibility of the porcine ECM-derived collagen scaffolds. Initial cell adhesion at 24 h was well maintained, with the Sponge+G group (0.24 ± 0.01) showing higher adhesion than the bare Sponge group ($p = 0.002$; Table 2, Figure 2A). At day 7, the Sponge+G group achieved a significantly enhanced cell proliferation ratio of 2.38 ± 0.13 fold compared to the non-loaded Sponge cohort ($p = 0.015$; Table 3, Figure 2C). In contrast, the day-7 relative metabolic activity ratio of the Sponge+G group was lower than that of the Sponge group (2.01 ± 0.41 vs. 2.89 ± 0.35; Table 2).

Similarly, the incorporation of gentamicin within the physically crosslinked framework did not impair cellular responses over the 7-day culture period. By day 7, the 3D-Phys+G group achieved a significant increase in cell proliferation, reaching a 4.39 ± 0.07 fold ratio ($p < 0.001$ vs. 3D-Phys; Table 3, Figure 2C). This rapid expansion was accompanied by a significantly deeper cell infiltration depth of 510.00 ± 82.81 µm compared to its non-loaded counterpart ($p = 0.004$ vs. 3D-Phys; Table 3, Figure 3A).

3.4. Scaffold Characterization and Gentamicin Content

SEM images of the 3D-Chem+G scaffold showed a regular grid structure with uniformly distributed pores, with pore opening dimensions ranging from 160 to 216 µm (194.0 ± 16.9 µm, eight measurements; Figure S1). The maximum tensile load was 8.29 ± 2.57 N ($n = 3$). The 3D-Chem+G scaffold showed no visible structural change after trypsin exposure ($n = 3$). During immersion in culture medium, the sponge scaffold began to disintegrate visibly at day 30 and had completely dissolved by day 80, whereas the 3D-printed scaffolds retained their overall shape through day 88 (Figure S2).

The microbiologically active gentamicin recovered from the 3D-Chem+G scaffold corresponded to 99.0% and 98.7% of the target loading at the high and low test concentrations, respectively, and the scaffold extract inhibited the growth of *S. epidermidis* ATCC 12228 to an extent comparable to that of the reference standard (Table S2).

4. Discussion

By integrating 3D bioprinting technology with two crosslinking methods and local antibiotic delivery, this study presents a potential strategy for the reconstruction of infected soft tissue defects. Our findings indicate that this construct has favorable preliminary cytocompatibility in vitro while retaining antibacterial activity. These findings are relevant to the clinical need for implantable biomaterials that can simultaneously support tissue regeneration and control local infection [3,4,11]. Specifically, this study showed three principal findings: 3D-printed scaffolds supported higher proliferation and deeper infiltration than conventional freeze-dried sponges; EDC/NHS chemical crosslinking was associated with higher day-7 relative metabolic activity than physical crosslinking; and gentamicin loading did not impair the cellular responses to the 3D-printed scaffolds, while active gentamicin was recovered from the scaffold.

One of the most notable findings of this study was that the 3D-printed scaffolds supported higher proliferation and substantially deeper cell infiltration than the sponge scaffolds, and most also showed higher initial adhesion; in contrast, the highest day-7 relative metabolic activity ratio was observed in the Sponge group. These differences may be related, at least in part, to the controlled pore architecture achieved through the layer-by-layer deposition process [17,18]. The grid pattern with alternating 0°/90° deposition directions created well-defined, interconnected pore channels (approximately 160–216 μm; Figure S1) that may facilitate nutrient diffusion and provide spatial guidance for cell migration. In contrast, sponge scaffolds prepared by freeze-drying exhibited a random pore structure that limited cell penetration primarily to the scaffold surface [9]. This difference was most evident in the cell infiltration data, where the 3D-printed groups achieved up to 3.37-fold greater penetration depth than sponge controls. However, because the sponge controls were not crosslinked, whereas both 3D-printed scaffold groups were, these differences cannot be attributed exclusively to 3D printing or pore architecture.

Regarding the crosslinking methods, our results suggest that chemical crosslinking may be favorable for maintaining cellular metabolic activity in this scaffold system. Specifically, the 3D-Chem and 3D-Chem+G groups maintained significantly higher metabolic activity at day 7 compared to the physically crosslinked groups (3D-Phys: $p = 0.040$ vs. 3D-Chem; 3D-Phys+G: $p < 0.001$ vs. 3D-Chem+G). At the molecular level, EDC/NHS chemistry forms stable, zero-length amide bonds by directly activating endogenous carboxyl groups of collagen to react with adjacent amine groups, which is generally reported to leave no cytotoxic crosslinker residues within the scaffold matrix [15,23]. We hypothesize that preservation of the native triple-helical conformation, which is required for integrin-mediated recognition of collagen through the GFOGER motif and related binding sequences [15,23], may contribute to the higher metabolic activity observed in the chemically crosslinked groups; however, collagen structure and integrin engagement were not directly assessed in this study.

In contrast, physical crosslinking via dehydrothermal treatment yielded a distinct cellular response profile characterized by rapid cellular expansion alongside altered metabolic kinetics. Constructs fabricated with physical crosslinking, particularly the 3D-Phys+G group, supported extensive cellular ingrowth and the highest proliferation rates at day 7, suggesting that vacuum thermal processing may maintain structural interconnectivity without chemical crosslinkers. The divergence between the highest relative BrdU incorporation and the lowest relative CCK-8 activity in the 3D-Phys+G group may reflect the different processes measured by these assays (DNA synthesis vs. dehydrogenase activity) and their separate normalization to day-0 values. The underlying mechanism, including possible thermal modification of the collagen matrix, was not determined in this study. Thus, the two crosslinking methods showed endpoint-dependent differences, and neither was uniformly

superior across all evaluated endpoints. The lower initial adhesion of the 3D-Chem+G group may be related to electrostatic interactions between polycationic gentamicin and functional groups on the EDC/NHS-activated collagen surface, which could temporarily mask integrin-binding motifs [10,23]; however, this possibility was not directly tested. By day 7, the 3D-Chem+G group showed metabolic activity, proliferation, and infiltration comparable to those of the non-loaded 3D-Chem group.

The microbiological assay showed that 98.7–99.0% of the target gentamicin loading was recovered in an active form after incorporation into the scaffold and subsequent processing, including freeze-drying and ethylene oxide sterilization. This loading (2 mg/cm^2) is equivalent to that of clinically used gentamicin–collagen sponges [26]. Previous clinical studies have demonstrated that gentamicin-collagen sponges can achieve local antibiotic concentrations exceeding the minimum inhibitory concentration for most clinically relevant pathogens, while maintaining systemic levels below toxic thresholds [4,27]. Therefore, the scaffold is expected to deliver gentamicin at locally effective concentrations, although release kinetics were not evaluated in this study. Future studies should include time-course drug release profiling and zone of inhibition testing against clinically relevant pathogens to fully characterize the antimicrobial performance.

Several limitations of this study should be acknowledged. First, the in vitro evaluation was performed using a single cell type (L929 mouse fibroblasts), and the results may not fully represent the complex cellular responses in vivo. Second, antibacterial evaluation was limited to a microbiological assay of gentamicin content, and release kinetics and efficacy against wound-associated pathogens were not assessed. Third, degradation was assessed only qualitatively, and biocompatibility beyond 7 days was not assessed. Fourth, this study did not include in vivo animal experiments to validate the scaffold's performance in a clinically relevant infected wound model. Fifth, because the sponge controls were not crosslinked, the independent contribution of 3D printing could not be separated from that of crosslinking. Sixth, physical characterization was limited to the 3D-Chem+G scaffold, and elastic modulus, compressive strength, porosity, and collagen structure were not assessed. Future investigations should address these limitations by incorporating human-derived cells, in vivo studies using infected wound models, and comprehensive drug release characterization.

5. Conclusions

Our findings indicate that the 3D-printed porcine ECM-derived collagen scaffold showed improved cellular performance compared with conventional freeze-dried sponges, with enhanced cell adhesion, proliferation, and infiltration, which may be related to its controlled pore architecture. Among the crosslinking methods evaluated, EDC/NHS chemical crosslinking was associated with higher day-7 metabolic activity than physical crosslinking, both with and without gentamicin, suggesting that it is a favorable manufacturing process for this scaffold. Importantly, gentamicin incorporation did not impair the cellular responses to the 3D-printed scaffolds, and 98.7–99.0% of the target loading was recovered as active gentamicin after the full fabrication and sterilization process, suggesting preserved antibacterial activity. These preliminary in vitro outcomes support the gentamicin-loaded, chemically crosslinked 3D-printed porcine ECM-derived collagen scaffold as a promising implantable biomaterial combining structural support for tissue regeneration with expected local antibacterial activity. Future in vivo studies using infected wound models will further elucidate its full therapeutic efficacy and accelerate its clinical translation.

Supplementary Materials: The following supporting information can be downloaded at: https://www.mdpi.com/article/10.3390/biomimetics11110834/s1, Figure S1: Scanning electron microscopy images of the 3D-Chem+G scaffold; Figure S2: Macroscopic appearance of the scaffolds during immersion in culture medium; Table S1: Cell infiltration depth measured in H&E-stained cross-sections; Table S2: Gentamicin content of the 3D-Chem+G scaffold determined by the microbiological assay.

Author Contributions: Conceptualization, M.J.K. and I.J.L.; methodology, M.J.K., H.G.K. and I.J.L.; formal analysis, M.J.K. and H.G.K.; investigation, M.J.K., H.G.K., S.H.H., E.H.H. and S.J.L.; data curation, S.H.H. and E.H.H.; writing—original draft preparation, M.J.K.; writing—review and editing, H.G.K. and I.J.L.; visualization, M.J.K. and S.J.L.; supervision, I.J.L.; project administration, I.J.L.; funding acquisition, I.J.L. All authors have read and agreed to the published version of the manuscript.

Funding: This work was supported by the Technology Development Program (S3373271), funded by the Ministry of SMEs and Startups (MSS, Korea). This research was supported by a grant of the Korea Health Technology R&D Project through the Korea Health Industry Development Institute (KHIDI), funded by the Ministry of Health & Welfare, Republic of Korea (RS-2026-25609784).

Institutional Review Board Statement: Not applicable. This study was an in vitro investigation performed with a commercially available L929 mouse fibroblast cell line and porcine-derived collagen supplied by a commercial manufacturer. It did not involve human participants, identifiable human material or data, or live animals; therefore, approval from the Institutional Review Board and the Institutional Animal Care and Use Committee was not required.

Informed Consent Statement: Not applicable.

Data Availability Statement: The data presented in this study are available on request from the corresponding author.

Conflicts of Interest: The authors declare no conflicts of interest. The funders had no role in the design of the study; in the collection, analyses, or interpretation of data; in the writing of the manuscript; or in the decision to publish the results.

References

1. Darouiche, R.O. Treatment of Infections Associated with Surgical Implants. *N. Engl. J. Med.* **2004**, *350*, 1422–1429. [CrossRef] [PubMed]
2. Seidelman, J.L.; Mantyh, C.R.; Anderson, D.J. Surgical Site Infection Prevention: A Review. *JAMA* **2023**, *329*, 244–252. [CrossRef] [PubMed]
3. ter Boo, G.J.A.; Grijpma, D.W.; Moriarty, T.F.; Richards, R.G.; Eglin, D. Antimicrobial Delivery Systems for Local Infection Prophylaxis in Orthopedic- and Trauma Surgery. *Biomaterials* **2015**, *52*, 113–125. [CrossRef] [PubMed]
4. Ruszczak, Z.; Friess, W. Collagen as a Carrier for On-Site Delivery of Antibacterial Drugs. *Adv. Drug Deliv. Rev.* **2003**, *55*, 1679–1698. [CrossRef] [PubMed]
5. Formanek, M.B.; Herwaldt, L.A.; Perencevich, E.N.; Schweizer, M.L. Gentamicin/Collagen Sponge Use May Reduce the Risk of Surgical Site Infections for Patients Undergoing Cardiac Operations: A Meta-Analysis. *Surg. Infect.* **2014**, *15*, 244–255. [CrossRef] [PubMed]
6. Kowalewski, M.; Pawliszak, W.; Zaborowska, K.; Navarese, E.P.; Szwed, K.A.; Kowalkowska, M.E.; Kowalewski, J.; Borkowska, A.; Anisimowicz, L. Gentamicin-Collagen Sponge Reduces the Risk of Sternal Wound Infections after Heart Surgery: Meta-Analysis. *J. Thorac. Cardiovasc. Surg.* **2015**, *149*, 1631–1640.e6. [CrossRef] [PubMed]
7. Chang, W.K.; Srinivasa, S.; MacCormick, A.D.; Hill, A.G. Gentamicin-Collagen Implants to Reduce Surgical Site Infection: Systematic Review and Meta-Analysis of Randomized Trials. *Ann. Surg.* **2013**, *258*, 59–65. [CrossRef] [PubMed]
8. Akkineni, A.R.; Spangenberg, J.; Geissler, M.; Reichelt, S.; Buechner, H.; Lode, A.; Gelinsky, M. Controlled and Local Delivery of Antibiotics by 3D Core/Shell Printed Hydrogel Scaffolds to Treat Soft Tissue Infections. *Pharmaceutics* **2021**, *13*, 2151. [CrossRef] [PubMed]
9. Loh, Q.L.; Choong, C. Three-Dimensional Scaffolds for Tissue Engineering Applications: Role of Porosity and Pore Size. *Tissue Eng. Part B Rev.* **2013**, *19*, 485–502. [CrossRef] [PubMed]
10. Singh, M.P.; Stefko, J.; Lumpkin, J.A.; Rosenblatt, J. The Effect of Electrostatic Charge Interactions on Release Rates of Gentamicin from Collagen Matrices. *Pharm. Res.* **1995**, *12*, 1205–1210. [CrossRef] [PubMed]
11. Badylak, S.F.; Freytes, D.O.; Gilbert, T.W. Extracellular Matrix as a Biological Scaffold Material: Structure and Function. *Acta Biomater.* **2009**, *5*, 1–13. [CrossRef] [PubMed]

12. Shoulders, M.D.; Raines, R.T. Collagen Structure and Stability. *Annu. Rev. Biochem.* **2009**, *78*, 929–958. [CrossRef] [PubMed]
13. Lee, C.H.; Singla, A.; Lee, Y. Biomedical Applications of Collagen. *Int. J. Pharm.* **2001**, *221*, 1–22. [CrossRef] [PubMed]
14. Chattopadhyay, S.; Raines, R.T. Review Collagen-Based Biomaterials for Wound Healing. *Biopolymers* **2014**, *101*, 821–833. [CrossRef] [PubMed]
15. Nair, M.; Johal, R.K.; Hamaia, S.W.; Best, S.M.; Cameron, R.E. Tunable Bioactivity and Mechanics of Collagen-Based Tissue Engineering Constructs: A Comparison of EDC-NHS, Genipin and TG2 Crosslinkers. *Biomaterials* **2020**, *254*, 120109. [CrossRef] [PubMed]
16. Haugh, M.G.; Jaasma, M.J.; O'Brien, F.J. The Effect of Dehydrothermal Treatment on the Mechanical and Structural Properties of Collagen-GAG Scaffolds. *J. Biomed. Mater. Res. A* **2009**, *89*, 363–369. [CrossRef] [PubMed]
17. Murphy, S.V.; Atala, A. 3D Bioprinting of Tissues and Organs. *Nat. Biotechnol.* **2014**, *32*, 773–785. [CrossRef] [PubMed]
18. Derakhshanfar, S.; Mbeleck, R.; Xu, K.; Zhang, X.; Zhong, W.; Xing, M. 3D Bioprinting for Biomedical Devices and Tissue Engineering: A Review of Recent Trends and Advances. *Bioact. Mater.* **2018**, *3*, 144–156. [CrossRef] [PubMed]
19. Lee, A.; Hudson, A.R.; Shiwarski, D.J.; Tashman, J.W.; Hinton, T.J.; Yerneni, S.; Bliley, J.M.; Campbell, P.G.; Feinberg, A.W. 3D Bioprinting of Collagen to Rebuild Components of the Human Heart. *Science* **2019**, *365*, 482–487. [CrossRef] [PubMed]
20. Crapo, P.M.; Gilbert, T.W.; Badylak, S.F. An Overview of Tissue and Whole Organ Decellularization Processes. *Biomaterials* **2011**, *32*, 3233–3243. [CrossRef] [PubMed]
21. Keane, T.J.; Swinehart, I.T.; Badylak, S.F. Methods of Tissue Decellularization Used for Preparation of Biologic Scaffolds and in Vivo Relevance. *Methods* **2015**, *84*, 25–34. [CrossRef] [PubMed]
22. Saldin, L.T.; Cramer, M.C.; Velankar, S.S.; White, L.J.; Badylak, S.F. Extracellular Matrix Hydrogels from Decellularized Tissues: Structure and Function. *Acta Biomater.* **2017**, *49*, 1–15. [CrossRef] [PubMed]
23. Davidenko, N.; Schuster, C.F.; Bax, D.V.; Farndale, R.W.; Hamaia, S.; Best, S.M.; Cameron, R.E. Evaluation of Cell Binding to Collagen and Gelatin: A Study of the Effect of 2D and 3D Architecture and Surface Chemistry. *J. Mater. Sci. Mater. Med.* **2016**, *27*, 148. [CrossRef] [PubMed]
24. Caruso, A.B.; Dunn, M.G. Functional Evaluation of Collagen Fiber Scaffolds for ACL Reconstruction: Cyclic Loading in Proteolytic Enzyme Solutions. *J. Biomed. Mater. Res. A* **2004**, *69*, 164–171. [CrossRef] [PubMed]
25. Ministry of Food and Drug Safety. *The Korean Pharmacopoeia*, 12th ed.; Ministry of Food and Drug Safety: Cheongju, Republic of Korea, 2019.
26. Bennett-Guerrero, E.; Ferguson, T.B.; Lin, M.; Garg, J.; Mark, D.B.; Scavo, V.A.; Kouchoukos, N.; Richardson, J.B.; Pridgen, R.L.; Corey, G.R. Effect of an Implantable Gentamicin-Collagen Sponge on Sternal Wound Infections Following Cardiac Surgery: A Randomized Trial. *JAMA* **2010**, *304*, 755–762. [CrossRef] [PubMed]
27. Friberg, Ö.; Jones, I.; Sjöberg, L.; Söderquist, B.; Vikerfors, T.; Källman, J. Antibiotic Concentrations in Serum and Wound Fluid after Local Gentamicin or Intravenous Dicloxacillin Prophylaxis in Cardiac Surgery. *Scand. J. Infect. Dis.* **2003**, *35*, 251–254. [CrossRef] [PubMed]

Disclaimer/Publisher's Note: The statements, opinions and data contained in all publications are solely those of the individual author(s) and contributor(s) and not of MDPI and/or the editor(s). MDPI and/or the editor(s) disclaim responsibility for any injury to people or property resulting from any ideas, methods, instructions or products referred to in the content.